Published by IOP Publishing for Sissa Medialab

Received: *September 12, 2019*
Revised: *November 18, 2019*
Accepted: *March 6, 2020*
Published: *April 14, 2020*

19TH International Symposium on Laser-Aided Plasma Diagnostics
22–26 September, 2019
Whitefish, Montana, U.S.A.

The distribution of OH in surface micro-discharge with different electrode widths by laser-induced fluorescence

Z. Wang,[a] C. Feng,[a] L. Gao[b] and H. Ding[a,1]

[a] *School of Physics, Key Laboratory of Materials Modification by Laser, Ion and Electron Beams, Chinese Ministry of Education, Dalian University of Technology, Dalian 116024, People's Republic of China*
[b] *Shanghai Institute of Ceramics, Chinese Academy of Sciences, Shanghai 200250, People's Republic of China*

E-mail: hding@dlut.edu.cn

Abstract: Cold atmospheric plasma has been successfully applied in the field of biomedicine. One of the most pressing challenge is the development of plasma devices, for example, large-area application in wound healing. Surface micro-discharge device is one new type of dielectric barrier discharge design with desirable plasma features, such as homogeneity over a large surface area. In this study, two devices with electrode width varying from 0.25 to 1.00 mm were fabricated. The contribution focuses on the impact of the hexagonal mesh electrode width on the degree of uniformity of hydroxyl (OH) radicals in the downstream region and the OH transport efficiency. Accordingly, OH radicals were measured as an indicator by laser-induced fluorescence. Steady state measurements of OH perpendicular to the dielectric surface demonstrated that narrow electrode width could not offer a high degree of uniformity, and will reduce the transport efficiency of reactive species.

Keywords: Plasma diagnostics - high speed photography; Plasma diagnostics - interferometry, spectroscopy and imaging

[1]Corresponding author.

https://doi.org/10.1088/1748-0221/15/04/C04033

Contents

2020 JINST 15 C04033

1 Introduction

Along with the research of cold atmospheric-pressure plasmas (CAPs), the research achievements promote many emerging applications and open new possibilities [1]. For the field of plasma medicine, it has received growing interest, such as wound healing [2] and cancer treatment [3]. Two key effects, inactivation of a broad spectrum of microorganisms and stimulation of cell proliferation and angiogenesis, are the foundation of cold atmospheric plasma applications in biomedical field [4]. These biomedical applications rely on the unique features of CAPs, namely, the plasma-initiated generation of reactive chemical species. These reactive chemical species generally play a vital role at lower concentration for living tissue, while they are considered to be harmful at larger concentration. Hence, the concentrations of species generated by plasma sources and treatment time (i.e., the dose) are key factors. Accordingly, the development of plasma devices is critical. Typically, Morfill et al. developed a new, very efficient, large area scalable and robust electrode design for the generation of reactive species, which was called surface micro-discharge (SMD) device [5]. The SMD electrode consists of a glass epoxy board, which is sandwiched by a copper foil layer and a mesh grid. As a kind of hybrid plasma sources, the SMD device combines the benefits of direct and indirect plasma sources [6]. In general, the plasma is generated on the dielectric surface from air or with noble gases. Owing to the physical separation between the plasma generation and the target, the low current does not pass through the target and ensures a safe application. Simultaneously, the separation causes a reduction in the flux of reactive species delivered to the target and limits the application efficacy [7]. Recent studies show that an electrohydrodynamic (EHD) body force (ionic wind) is responsible for the transport of reactive species from the dielectric surface and forms a vertical jet [8, 9]. The directional transport can enhance the delivery of these species.

In the work, OH radical was measured as an indicator. Two SMD devices with electrode width varying from 0.25 to 1.00 mm were fabricated with a specified edge to edge spacing of 4.0 mm. We investigated the impact of the electrode width on the degree of uniformity of OH radicals in the downstream region and the transport efficiency induced by ionic wind.

2 Experimental setup

The SMD electrode used in this study was constructed by printed circuit board technique. Figure 1 shows the front and the back views of the SMD device. The discharge device consisted of a three-layer structure, including two 30 µm thickness copper-tin layers, which were attached either side of a 1.6 mm thick glass epoxy (FR-4) substrate as powered electrode and grounded electrode, respectively. The grounded electrode has a hexagonal lattice structure, and was exposed to a surrounding gas. The specified edge to edge spacing was fixed at 4.00 mm within one mesh hexagon and the electrode width w was varied from 0.25 to 1.00 mm. On the opposite side of the dielectric board, the high voltage (HV) electrode was a planar plate of $35 \times 33\,\mathrm{mm}^2$, and buried with acrylic resin to avoid the formation of plasma on this side.

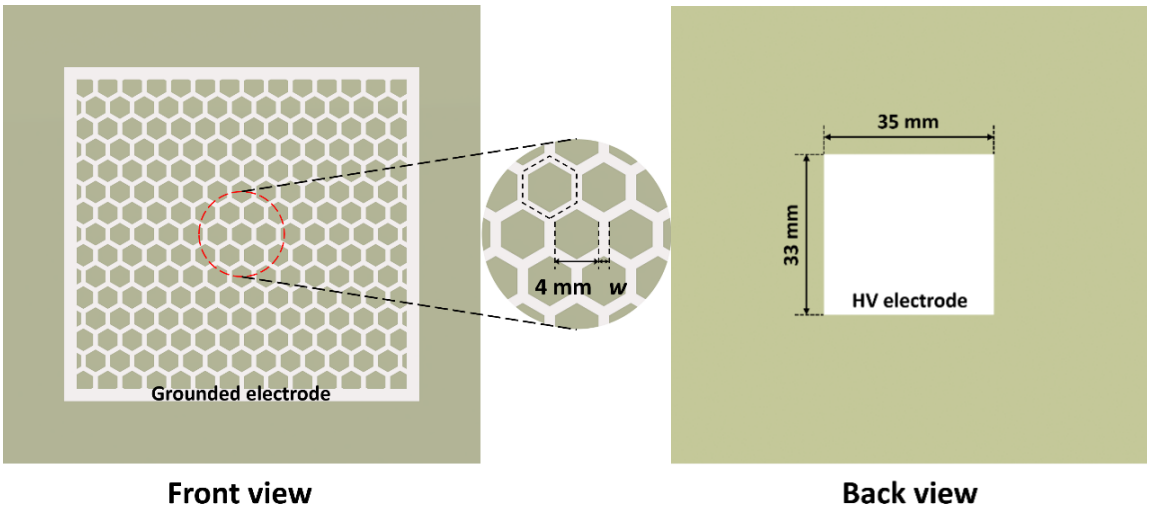

Figure 1. The front and back views of the surface micro-discharge device used in this study.

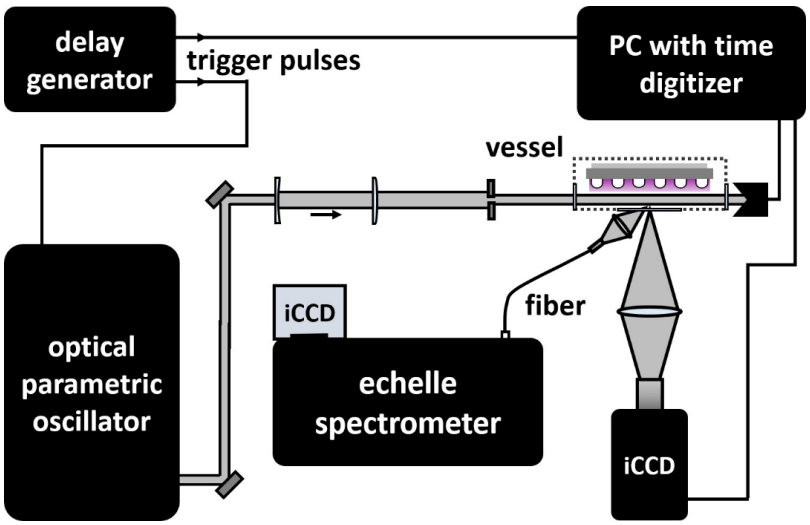

Figure 2. Schematic of the experimental setup for LIF and OES measurements.

2020 JINST 15 C04033

The two SMD devices were powered by a sinusoidal voltage with peak-to-peak voltage of 5.0 kV at a frequency of 30 kHz in modulated mode. The applied voltage and discharge current were monitored by a HV probe (Tektronix P6015A) and a current probe (Pearson 2877). The waveforms were recorded by an oscilloscope (LeCroy WaveSurfer 42Xs). The averaged dissipated power was determined using the mean of the production between the applied voltage and current over 30 cycles. The SMD device was placed inside a quartz box. Helium (99.995% purity) was fed into the box with a constant flow rate of 1.5 SLM through a mass flow controller (Aalborg GFC17).

The laser-induced fluorescence (LIF) measurements were carried out with a tunable optical parametric oscillator (Ekspla NT-342C-SH), pumped with Nd:YAG laser at 355 nm and a repetition rate of 10 Hz (see figure 2) [9]. The laser beam was expanded to a sheet using a horizontally concave lens and a vertically convex lens. The energy of the Gaussian laser sheet entering the box is about 0.26 mJ, and the nominal bandwidth is 5.02 cm^{-1}. In this study, the laser excitation wavelength was set to 281.90 nm. The laser excites the OH $X^2\Pi(v = 0) \rightarrow A^2\Sigma^+(v = 1)$ transition. The measured LIF spectrum is around 315 nm, which corresponds to the transition $A^2\Sigma^+(v = 1) \rightarrow X^2\Pi(v = 1)$ and $A^2\Sigma^+(v = 0) \rightarrow X^2\Pi(v = 0)$. The fluorescence was collected by an iCCD camera (Princeton Instrument PIMAX 4).

3 Results and discussion

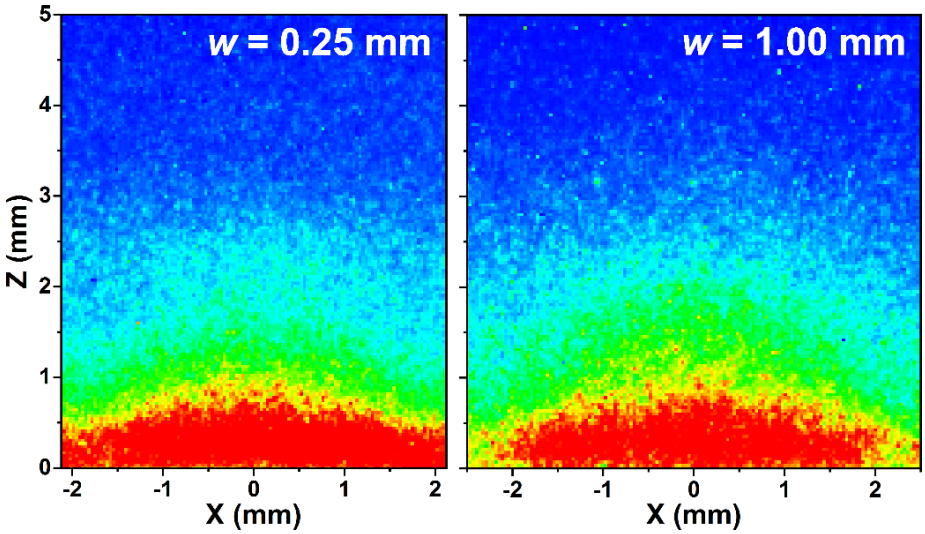

Figure 3. Spatial distribution of OH radicals in a direction perpendicular to the dielectric surface for various lattice widths at a constant lattice distance of 4 mm and a constant applied voltage of 5 kV.

On application of a peak-to-peak voltage of 5.0 kV, the electric field generates a discharge resulting in plasma near the dielectric. The gas temperature is about 320 ± 15 K in $w = 0.25$ and 1.00 mm cases through the fitting of the OH($A - X$) spectrum using LIFBASE [10]. Theoretically, the quantity, distribution, fractional abundance of rotational state and spatial distribution of rotational temperature should be considered when the LIF intensity is employ to represent the distribution of the relative OH density. In this study, the error caused by the variation of rotational temperature is about 3% by calculating the excitation cross section, which is the convolution of the laser and the absorption

2020 JINST 15 C04033

spectrum. Therefore, the distribution of the LIF intensity was used to represent the distribution of the relative OH density. Previous works have studied the species transport in surface dielectric barrier discharges using computational modelling and experimental measurements [8, 9, 11, 12]. For hexagonal SMD device, plasmas originate close to the edge of the electrode and propagate towards the mesh center driven by ionic wind. Whereafter, a wall jet was formed perpendicular to the dielectric surface [9, 13]. As shown in figure 3, the spatial distribution of OH radicals are demonstrated in the steady state operation for electrode widths of w = 0.25 and 1.00 mm, respectively. It is clear that the ground state OH(X) radicals are mainly distributed in the vicinity of the dielectric surface and decrease with increasing the distance from the surface. From figure 3, the variation in electrode width has no significant impact on the length of the jet. In addition, one can observe that the decrease of electrode width could not offer a high degree of uniformity in the downstream region. It is clear that the OH intensity in the region above the rim electrode is higher when the electrode width is 0.25 mm compared to the 1.00 mm case. Besides, a strong OH signal can be detected up to a distance of 3 mm from the device surface. To provide further comparison of the spatial distribution, the normalized intensity profile of OH radicals from the dielectric surface to 5 mm is plotted in figure 4. It is found that the normalized intensities have no significant difference in the region between 0 and 1 mm. Visible plasma is located only near the dielectric surface with a few hundreds of microns thick. In addition, with an electrode width of 1.00 mm, the OH intensity is higher in the region between 1–3 mm.

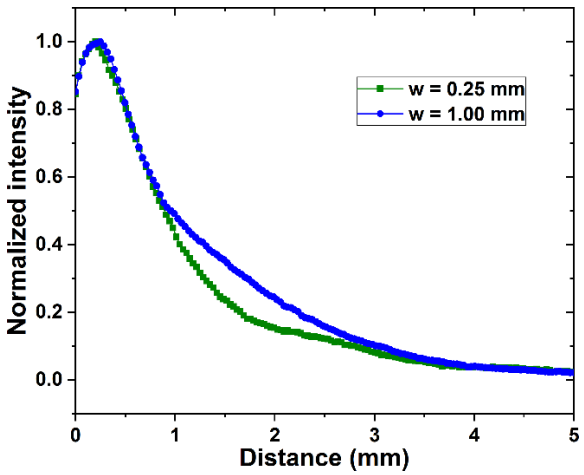

Figure 4. The normalized OH intensity as a function of space for various lattice widths.

To better understand the difference of the spatial profiles of OH, the emission patterns were captured under the same experimental conditions as examined in figures 3 and 4. Figure 5 demonstrates the emission patterns of the SMD within a single mesh cell for electrode widths of 0.25 mm and 1.00 mm. The time integrated false color images were extracted along the midline of the hexagonal mesh electrode according to the dash hexagon marked in the magnified device image in the red dotted circular frame in figure 1. The solid white hexagon indicates the inner boundary of the mesh electrode. The outside of the white hexagon is the grounded electrode. With the electrode width of 1.00 mm, there is no interaction between two individual neighbouring meshes, and the plasma is found to cover the entire electrode area with strong emission intensity. However, for the narrow width

2020 JINST 15 C04033

of 0.25 mm, two individual plasmas connect over the rim electrode, and the strong emission regions only exist in neighborhood of hexagonal sides. Previous study indicated that the charges produced in the discharge lead to an accumulation and form ion cloud close to rim electrode above the surface [14]. These charges build up an electric field, leading to a reduction in the electric field between the exposed electrode and the mesh center and a subsequent decrease in the movement of charged species drifting in the electric field. When the electrode width of the rim electrode w is 0.25 mm, the concentration of charged species is higher than the 1.00 mm case. Therefore, the field generated by charged species has a greater influence on the small scale device, resulting in a decline in the ionic wind efficiency. In the 0.25 mm case, hence, OH radicals are mainly located in the vicinity of the dielectric surface with a low concentration in the adjacent downstream region, shown in figure 4.

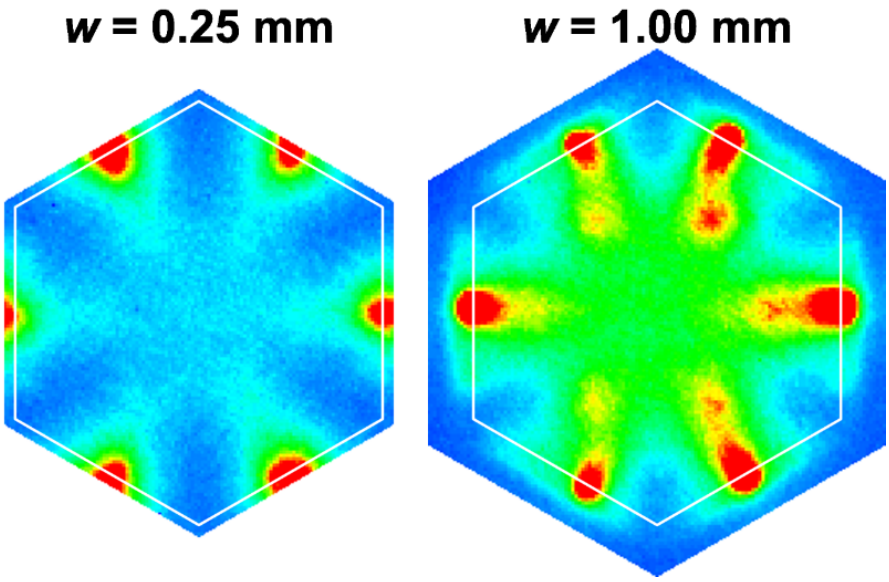

Figure 5. Luminous patterns of the SMD during one cycle for two electrode widths.

4 Conclusion

In this study, the influence of the hexagonal mesh electrode width on the degree of uniformity of OH radicals in the downstream region and the OH transport efficiency were investigated by laser-induced fluorescence. Steady state measurements of OH perpendicular to the dielectric surface demonstrated that narrow electrode width could not offer a high degree of uniformity, and will reduce the transport efficiency of OH radicals.

Acknowledgments

This work was supported by the National Natural Science Foundation of China (Nos. 51837008 and 11705021), the National Key R&D Program of China (No. 2017YFE0301304) and the Fundamental Research Funds for the Central Universities (Nos. DUT19LK07, DUT18LK31 and DUT18LK38).

2020 JINST 15 C04033

References

[1] Y. Akishev, Z. Machala and N. Koval, *Special issue on recent developments in plasma sources and new plasma regimes*, *J. Phys.* **D 52** (2019) 130301.

[2] D.W. Kim, T.J. Park, S.J. Jang, S.J. You and W.Y. Oh, *Plasma treatment effect on angiogenesis in wound healing process evaluated in vivo using angiographic optical coherence tomography*, *Appl. Phys. Lett.* **109** (2016) 233701.

[3] M. Vandamme, E. Robert, S. Lerondel, V. Sarron, D. Ries, S. Dozias et al., *ROS implication in a new antitumor strategy based on non-thermal plasma*, *Int. J. Cancer* **130** (2011) 2185.

[4] S. Bekeschus, P. Favia, E. Robert and T. von Woedtke, *White paper on plasma for medicine and hygiene: Future in plasma health sciences*, *Plasma Proc. Polym.* **16** (2018) 1800033.

[5] G.E. Morfill, T. Shimizu, B. Steffes and H.-U. Schmidt, *Nosocomial infections—a new approach towards preventive medicine using plasmas*, *New J. Phys.* **11** (2009) 115019.

[6] G. Isbary, T. Shimizu, Y.-F. Li, W. Stolz, H.M. Thomas, G.E. Morfill et al., *Cold atmospheric plasma devices for medical issues*, *Expert Rev. Med. Devices* **10** (2013) 367.

[7] P. Olszewski, J. Li, D. Liu and J. Walsh, *Optimizing the electrical excitation of an atmospheric pressure plasma advanced oxidation process*, *J. Hazard. Mater.* **279** (2014) 60.

[8] M. Taglioli, A. Shaw, A. Wright, B. FitzPatrick, G. Neretti, P. Seri et al., *EHD-driven mass transport enhancement in surface dielectric barrier discharges*, *Plasma Sources Sci. Technol.* **25** (2016) 06LT01.

[9] Z. Wang, C. Feng, L. Gao and H. Ding, *The transport behaviour of OH radicals in atmospheric pressure surface micro-discharge*, *J. Phys.* **D 52** (2019) 105203.

[10] J.Luque and D.R. Crosley,*Lifbase: database and spectral simulation program*, *SRI International Report MP* **99** (1999) 009.

[11] M.I. Hasan and J.L. Walsh, *Numerical investigation of the spatiotemporal distribution of chemical species in an atmospheric surface barrier-discharge*, *J. Appl. Phys.* **119** (2016) 203302.

[12] M.I. Hasan and J.L. Walsh, *Influence of gas flow velocity on the transport of chemical species in an atmospheric pressure air plasma discharge*, *Appl. Phys. Lett.* **110** (2017) 134102.

[13] A. Dickenson, N. Britun, A. Nikiforov, C. Leys, M.I. Hasan and J.L. Walsh, *The generation and transport of reactive nitrogen species from a low temperature atmospheric pressure air plasma source*, *Phys. Chem. Chem. Phys.* **20** (2018) 28499.

[14] Y. Lagmich, T. Callegari, T. Unfer, L.C. Pitchford and J.P. Boeuf, *Electrohydrodynamic force and scaling laws in surface dielectric barrier discharges*, *Appl. Phys. Lett.* **90** (2007) 051502.

2020 JINST 15 C04033